Biosensors and Bioelectronics 123 (2019) 230–236

Contents lists available at ScienceDirect

Biosensors and Bioelectronics

journal homepage: www.elsevier.com/locate/bios

Highly sensitive olfactory biosensors for the detection of volatile organic compounds by surface plasmon resonance imaging

Charlotte Hurot[a], Sophie Brenet[a], Arnaud Buhot[a], Emilie Barou[b], Christine Belloir[b], Loïc Briand[b], Yanxia Hou[a,*]

[a] Uni. Grenoble Alpes, CEA, CNRS, INAC-SyMMES, 17 Rue des Martyrs, 38000 Grenoble, France
[b] INRA, CNRS, Université de Bourgogne – Franche Comté, Centre des Sciences du Goût et de l'Alimentation, 17 rue Sully, 21000 Dijon, France

ARTICLE INFO

Keywords:
Odorant binding proteins
Olfactory biosensor
Surface plasmon resonance imaging
Volatile organic compound

ABSTRACT

Nowadays, monitoring of volatile organic compounds (VOCs) is very important in various domains. In this work, we aimed to develop sensitive olfactory biosensors using odorant binding proteins (OBPs) as sensing materials. Three rat OBP3 derivatives with customized binding properties were designed and immobilized on the same chip for the detection of VOCs in solution by surface plasmon resonance imaging (SPRi). We demonstrated that the proteins kept their binding properties after the immobilization under optimized conditions. The obtained olfactory biosensors exhibited very low limits of detection in both concentration (200 pM of β-ionone) and in molecular weight of VOCs (100 g/mol for hexanal). Such a performance obtained with SPRi in solution is especially remarkable. We hypothesized that the binding of VOCs to the active sites of OBPs induced a local conformational change in the proteins. This change would give rise to a variation of refractive index, to which SPRi is extremely sensitive. In addition, the olfactory biosensors showed a high selectivity especially at relatively low VOC concentrations. With optimized regeneration procedures, they also showed very good repeatability not only from measurement to measurement but also from chip to chip with a lifespan up to almost two months. These olfactory biosensors are particularly interesting for trace detection of VOCs in solution.

1. Introduction

Volatile organic compounds (VOCs) are the major components of odors and abound in our environment. Over the past decades, the monitoring of VOCs has become an important concern in several domains including environment for on-field air quality control, industrial manufacturing process for the quality control of beverages, food and cosmetics, public safety, and healthcare for disease diagnosis. Classical analytical methods such as gas chromatography coupled to mass spectroscopy, although reliable and accurate, are often time-consuming and require expensive equipment and skilled staff. To meet this growing need, sensors inspired from the biological nose such as electronic noses have been developed. Most of them are based on a combination of few non-specific sensing materials such as metal oxides or polymers (Chiu and Tang, 2013). Although these systems have good sensitivity, they generally lack selectivity between VOCs. Consequently, their ability to discriminate between odors in complex media can be compromised.

Thanks to great progress in the field of biology, genetic engineering and biotechnology, it is now possible to use biological materials as receptors, including whole tissues and cells (Hou et al., 2012a; Lee et al., 2015; Liu et al., 2010). These bio-receptors are very promising for the analysis of VOCs with a high sensitivity and selectivity (Wasilewski et al., 2017, 2018). However, the main difficulties are related to their stability. Besides, olfactory cells or nanovesicles are hard to manufacture and manipulate. In literature, two families of proteins from the olfactory system of animals have particularly garnered attention for their role in the design of olfactory biosensors: olfactory receptors (ORs) (Du et al., 2013; Gomila et al., 2006; Hou et al., 2007) and odorant binding proteins (OBPs) (Barou et al., 2015; Hou et al., 2005; Kotlowski et al., 2018; Lu et al., 2017c; Manai et al., 2014). However, for membrane proteins such as ORs, their stability and functions can be easily lost after their immobilization onto a sensor. Moreover, their mass production and purification are still very complicated today. In contrast, OBPs are ideal candidates for such applications. (Pelosi et al., 2014). First, they are stable to temperature and pH change, organic solvents and proteolytic digestion. Second, they are soluble and thus easy to produce and purify. Finally, their binding properties can be tailored through site-directed mutagenesis.

Vertebrate OBPs are small soluble proteins of the lipocalin family (~ 20 kDa), highly secreted in the olfactory mucus covering the olfactory

* Corresponding author.
E-mail address: yanxia.hou-broutin@cea.fr (Y. Hou).

https://doi.org/10.1016/j.bios.2018.08.072
Received 30 June 2018; Received in revised form 27 August 2018; Accepted 29 August 2018
Available online 31 August 2018
0956-5663/

epithelium. They have a calyx structure with eight beta-sheets forming a hydrophobic binding pocket, in which they reversibly bind VOCs with dissociation constants in the micro-molar range (Heydel et al., 2013). Although the physiological role of OBPs is not completely elucidated, one of their speculated functions is to transport VOCs through the aqueous mucus, release them to ORs, and even facilitate their interaction with ORs. In rats, three OBP subtypes have been identified with complementary binding spectra (Löbel et al., 2002). Rat OBP1 binds with heterocyclic compounds such as pyrazine derivatives, OBP2 is specific for aliphatic aldehydes and carboxylic acids, while OBP3 interacts with VOCs possessing saturated and unsaturated ring structures. Herein, OBP3 was chosen as a base to design three different recombinant proteins. The amino acid residues composing the binding pocket of the rat OBP3 were modified to create synthetic OBPs with varied binding properties. To date, only a very few olfactory biosensors described in literature used more than one kind of OBP. Di Pietrantonio and colleagues used a combination of two bovine and one porcine OBP (Di Pietrantonio et al., 2013), and Kotlowski and collaborators made slight modifications of an insect OBP to improve its orientation and rigidity (Kotlowski et al., 2018) To our knowledge, this is the first time that custom-made OBPs with controlled binding properties are used for the development of olfactory biosensors.

So far, different transduction techniques have been used to develop OBP-based olfactory biosensors, including electrochemical impedance (Hou et al., 2005; Lu et al., 2016), field-effect or capacitance-modulated transistors (Kotlowski et al., 2018; Larisika et al., 2015; Mulla et al., 2015), localized surface plasmon resonance (Zhang et al., 2015), microcantilevers (Manai et al., 2014), surface acoustic wave (SAW) (Di Pietrantonio et al., 2013), and solidly mounted resonators (Cannatà et al., 2012). These studies showed that OBPs are stable and active after the immobilization and the obtained biosensors are efficient for VOC analysis. It is noteworthy that in literature, none of the OBP-based biosensors utilized surface plasmon resonance imaging (SPRi) for the detection of VOCs. However this optical transduction method has been widely applied for the development of biosensors and biochips, allowing in real-time, label-free and high-throughput monitoring of binding events (Daniel et al., 2013; Homola, 2008; Lu et al., 2017a; Maillart et al., 2012; Wang et al., 2010). SPRi is generally considered unsuitable and limited for the analysis of low-weight molecules such as VOCs (molecular weight < 300 g/mol). Interestingly, some previous studies showed that the binding of VOCs might induce local conformational changes in OBPs (Hajjar et al., 2006; Nespoulous et al., 2004). Herein, this phenomenon will be used to challenge the analysis of VOCs by SPRi in solution. The idea is to immobilize OBPs in the close proximity of the SPRi prism through self-assembly without using an intermediate layer and cross-linker. In this way, their conformational change is expected to give rise to a variation of local refractive index, to which SPRi is very sensitive (Gestwicki et al., 2001).

In this study, three derivatives of OBP3 were used with customized binding properties for VOCs of interest. In addition, a cysteine was added at the N-terminal end for their direct immobilization on the gold surface of a prism by self-assembly. The proteins were immobilized on the same chip in a microarray format, and their density on the chip was optimized. The efficiency of SPRi for VOC sensing in solution was assessed using three VOCs. Finally, the performances of the obtained olfactory biosensors were evaluated in terms of sensitivity, selectivity, repeatability and stability.

2. Materials and methods

2.1. Materials

Potassium nitrate (KNO_3), sodium dihydrogen phosphate (NaH_2PO_4), sodium acetate (CH_3CO_2Na), glycerol and acetonitrile were purchased from Sigma Aldrich. β-ionone (> 97%), hexanoic acid (> 98%), and hexanal (> 95%) were also bought from Sigma Aldrich. Methanol and ethanol were provided by Thermofisher and water was provided by Carlo Erba. All the solvents were HPLC-MS grade to avoid any possible contamination by undesired VOCs that may block the binding sites of OBPs.

Three derivatives of the third rat odorant binding protein (OBP3) were used in this work, including a “wild type” protein (OBP3-w), and two modified proteins named OBP3-a and OBP3-c. The binding properties of these proteins were customized by modifying the amino acid residues of their binding pockets. In addition, a cysteine was included at the N-terminal end of the three OBPs to enable their immobilization by self-assembly on the gold surface of a prism. The general method used for the production, purification and characterization of such recombinant proteins was previously described in (Barou et al., 2015) and are briefly summarized in the following. The recombinant His-tagged proteins were expressed using *Escherichia coli*. The purification of the proteins was performed using immobilized metal affinity chromatography (IMAC). The protein purity was assessed by SDS-PAGE. The binding properties of the three OBPs for different VOCs were measured using isothermal titration microcalorimetry (ITC) at 25 °C, which revealed a 1:1 stoichiometry for binding.

2.2. Preparation of protein microarray

The three OBPs were immobilized in a microarray format onto a prism covered with a thin gold layer (SPRi-Biochip, Horiba Sci, Orsay, France). The gold surface of the prism was cleaned 48 h before functionalization, with a Femto plasma cleaner (Diener Electronic, Germany) for 3 min using these parameters: 75% oxygen, 25% argon, 0.6 mbar, 40 W. Then, droplets of 6 nL of proteins in phosphate buffer (50 mM NaH_2PO_4, pH 7.5) with 5% (v/v) glycerol were deposited on the prism by a non-contact spotting robot (sciFLEXARRAYER, Scienion, Germany). In this study, for each OBP, spotting solutions at four different concentrations (2 µM, 4 µM, 8 µM and 16 µM) were used and compared in order to optimize the protein density on the chip. Moreover, for each condition, six replicates were randomly deposited on the prism to avoid any bias due to the position effect on the microarray. In this way, 72 biosensors in total were integrated on the same prism.

Afterwards, the prism was placed in a humidity-controlled chamber (relative humidity of 96%) at 4 °C overnight for the immobilization of the proteins by self-assembly. Finally, the prism was rinsed thoroughly with phosphate buffer to eliminate unfixed OBPs, and stored in phosphate buffer, at 4 °C, before use.

2.3. Analysis of VOCs by SPRi

The detection of VOCs was performed using a commercial SPRi apparatus (Horiba Scientific) placed in an incubator at 25 °C. A collimated, polarized light beam at 663 nm was sent through the prism to illuminate the whole microarray. The analysis of VOCs was achieved at a fixed working angle. Upon the injection of VOCs, the variations of reflectivity for all the spots were simultaneously monitored and recorded with a CCD camera, with each pixel mapping a specific position on the prism. A measurement was taken every three seconds.

The detailed setup was described previously (Hou et al., 2014, 2012b). The prism with immobilized OBPs was mounted into a 10 µL PEEK flow cell with hexagonal shape. This cell was connected to a fluidic system. Running buffer (50 mM NaH_2PO_4, pH 7.5) was pushed in the PEEK tubing by a computer-controlled syringe pump (Cavro Scientific Instruments, USA) at a constant flow of 1.56 µL/s. It was filtered beforehand and passed through a degassing system (Alltech, France) before arrival in the flow cell to avoid dust and air bubbles.

Prior to each experiment, all the tubing was rinsed carefully with methanol and water to ensure that no pollutant would remain from previous experiments. Before any VOC sample injection, a blank injection of running buffer was systematically performed to control the

Table 1
Characteristics of the three VOCs used in this study and their respective dissociation constants at equilibrium with OBP3-w and OBP3-a, determined in solution by ITC.

Odorant	Skeletal formula	Molecular weight ($g.mol^{-1}$)	K_d with OBP3-w (μM)	K_d with OBP3-a (μM)
β-ionone	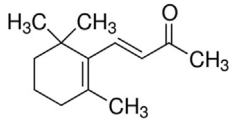	192.3	0.18	0.52
Hexanoic acid	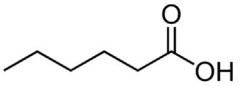	116.16	* Negative control	* Negative control
Hexanal	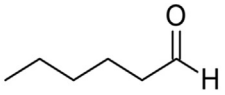	100.16	4.6	0.026

cleanliness of the fluidic system. VOC samples were prepared by diluting pure products in the filtered running buffer. Then, they were manually injected through a six-port injection valve (Upchurch Sci., USA) using a syringe. The volume of the injection loop was 1 mL or 2 mL. Under these conditions, it took approximately 4 min between the injection and the moment the VOC samples reached on the prism, and around 10 min to complete an injection. Furthermore, β-ionone, selected as a reference compound, was injected systematically at the beginning and the end of any session in order to assess the functionality and stability of the chip with time.

2.4. Regeneration process

After the injection of β-ionone at low concentrations (< 800 pM), the regeneration was completed simply by keeping the buffer solution running for additional 30 min. After an injection of β-ionone at higher concentration (> 800 pM) or after the injection of hexanal, another regeneration strategy was needed. In this case, the running buffer was changed to acetate buffer (CH_3CO_2Na at 50 mM, pH 7.5). Then, three successive injections were performed using 20% ethanol (v/v) in acetate buffer, and then 30% acetonitrile (v/v) in acetate buffer, twice. All the procedure was performed in situ with the chip mounted on the SPRi setup, with an optimal flow rate of 1.04 μL/s.

2.5. Data analysis

For an easy comparison, all the curves were brought to zero at the beginning of an injection by subtracting the respective mean reflectivity measured for 1 min before the VOC injection. Then, assuming that the drift was linear with time, it was evaluated and subtracted to the signal for each spot. The signals obtained on the 6 replicate spots of OBPs were averaged, and a standard error was calculated between them. The average reflectivity given by the spots of OBP3-c, used as negative control, was subtracted to the signals of OBP3-w and OBP3-a at all time. It allowed to get rid of refractive index variation effects. These effective signals are given in percentage of variation of reflectivity (Δ%R). They were used for the calculation of the signal to noise ratio (SNR). A one-minute rolling average was performed on the curves presented herein.

The noise value was calculated using the following equation, with *StdError* the standard error calculated between the *n* replicates.

$$Noise = \frac{StdError}{\sqrt{n}}$$

In this way, the calculated value gives a direct indication of the repeatability between replicates on the same chip. All the experiments presented thereafter were performed on at least three different chips.

The SNR was then calculated by dividing the effective signal by the noise. The effective signals obtained with OBP3-w and OBP3-a were considered valid if the SNR was above three.

3. Results and discussion

As mentioned before, in this study, three OBP derivatives of the third rat odorant binding protein OBP3 were used. Their binding properties were customized by modifying the amino acid residues of their binding pockets. The engineering and the characterization of these particular derivatives of OBPs will be published elsewhere. The “wild type” protein (OBP3-w) corresponds to the natural OBP3. The OBP3-a variant was designed by introducing a lysyl residue in the binding pocket. This modification was inspired by the human OBP, to which this residue confers a higher affinity for aldehydes through the formation of H-bond with the added amine function (Tcatchoff et al., 2006). Thus, the affinity of OBP3-a towards aldehydes is improved. For the last derivative OBP3-c, bulky amino acids were introduced in its binding pocket. Consequently, the binding site is cluttered and it is incapable of binding any VOCs. Herein, it was used for negative control.

Three VOCs were tested: β-ionone, hexanoic acid and hexanal. Their characteristics are presented in Table 1. β-ionone is an aroma compound found in a variety of essential oils, contributing significantly to the odor of violets and the taste of raspberries. It can bind to both OBP3-w and OBP3-a but with a higher affinity for OBP3-w. It was chosen as the reference VOC during all experiments. On the contrary, hexanal whose scent resembles that of freshly cut grass was shown to bind preferentially to OBP3-a in solution. As for hexanoic acid, a carboxylic acid with a fatty and cheesy odor, did not bind to any of the three recombinant proteins during ITC tests. It was, therefore, used as a negative control. The analysis of these three VOCs would allow us to assess the activity of the proteins after their immobilization on the prism as well as the sensitivity and selectivity of the obtained olfactory biosensors.

3.1. Optimization of OBP density after immobilization on the microarray

The density of OBPs grafted on the microarray is a key point. It may have influence on the binding properties of the proteins as well as on the signal intensity. It is related to the concentration of OBPs in the spotting solution and the conditions under which the self-assembly of proteins takes place. In an ideal case, the proteins would form a well-organized monolayer with their binding pockets pointing upwards to facilitate the access of VOCs. If the density of OBPs is too low, the

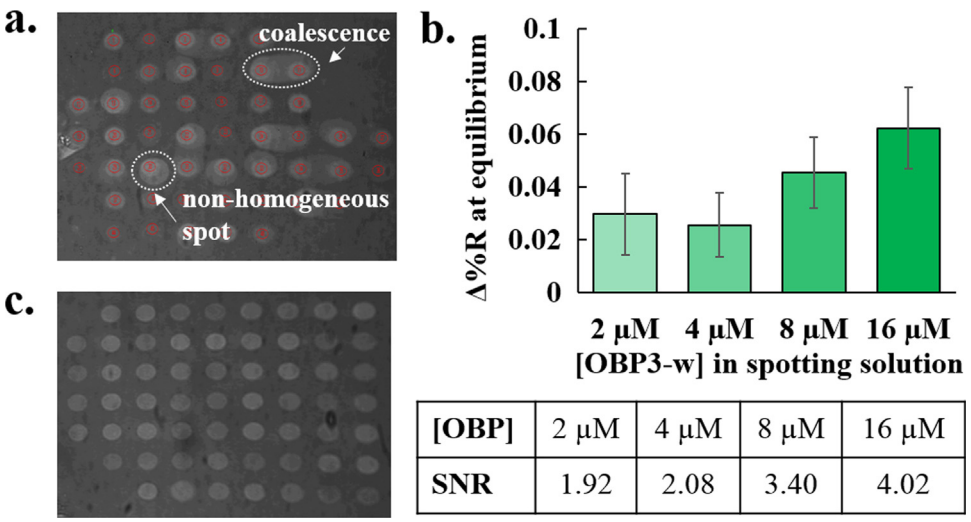

[OBP]	2 µM	4 µM	8 µM	16 µM
SNR	1.92	2.08	3.40	4.02

Fig. 1. a) SPR image of the microarray after self-assembly of the OBPs at different concentrations (2 µM, 4 µM, 8 µM and 16 µM), showing non-uniform spots. Red circles define the regions of interest, where the interactions with VOCs are followed and analyzed. b) Effective signals obtained with OBP3-w immobilized at the four different concentrations and after exposure to β-ionone (200 pM). The corresponding SNR values are presented in the table below. c) An SPR image of all the spots obtained after self-assembly of OBPs with the optimized concentration (8 µM). (For interpretation of the references to color in this figure legend, the reader is referred to the web version of this article.)

adsorbed quantity of VOC will be low. It could be critical for the analysis of small VOCs by SPRi, often considered as an optical scale. Furthermore, in this case, the gold surface may not be completely blocked, allowing the VOCs to adsorb non-specifically onto it. On the contrary, if the concentration of protein is too high, the formation of additional disordered layers could be favored. In this case, the proteins on the top layer would have random orientation and may block access to the binding sites of the proteins in the underlayer. Moreover, it would be difficult to prepare reproducible biosensors under such conditions.

To optimize the density of OBPs, four concentrations of OBP3-w and OBP3-a (2 µM, 4 µM, 8 µM and 16 µM) were tested in the spotting solution. As shown in the SPR image (Fig. 1a), the spots obtained after protein self-assembly at different concentrations are not identical. For the highest concentration at 16 µM, non-homogeneous spots with a halo and even coalescence with other spots nearby were observed. It is likely that at this concentration additional disordered layers were formed. During the storage of the prism in phosphate buffer, the proteins from the top layer tend to spread and self-assemble around the spot to form the halo.

Furthermore, when the microarray was put in contact with β-ionone at 200 pM (Fig. 1b) the SNR were both below 3 for the spots of OBP3-w deposited at 2 µM and 4 µM. Thereby, these signals were considered as unreliable, probably due to too low density of OBPs as mentioned earlier. For all the spots of OBP3-w deposited at 8 µM and 16 µM, the SNR was above 3. Thus, in both cases the signals were valid.

Taking into account these two observations, we assumed that at 8 µM, a dense monolayer was formed, since an additional layer would have spread around like at 16 µM, and a monolayer not dense enough would have led to a weaker signal. Thus, the microarray was prepared using spotting solutions at 8 µM for all the OBPs for the following study. Satisfyingly, under this condition, all the spots were dense, homogeneous and uniform (Fig. 1c), with an estimated density of 6×10^{12} proteins/cm^2.

3.2. VOC sensing by SPRi

The three VOCs (β-ionone at 68 nM, hexanal at 2.3 µM, hexanoic acid at 680 nM) were successively injected onto the microarray. The interaction between each VOC and the three OBPs were simultaneously monitored by SPRi. The effective kinetic responses for the biosensors based on OBP3-w and OBP3-a are presented in Fig. 2. For example, with β-ionone at 68 nM (Fig. 2a), nothing happened during the first 4 min following the injection. It corresponds to the time needed for the sample to go through the injection valve and reach the microarray. As soon as the sample came into contact with the olfactory biosensors, the reflectivity of the spots of OBP3-w and OBP3-a increased and reached equilibrium about 10 min after the injection.

In order to confirm that these signals resulted from the binding of VOCs to OBPs rather than optical sensitivity differences between the spots of different protein derivatives, hexanoic acid (negative control) was injected and analyzed. Indeed, in practice, any injection of VOCs induced a slight shift in refractive index, which, in this case, could result in different variations of reflectivity. Satisfyingly, in Fig. 2b, no increase of signals was observed. OBP3-w and OBP3-a were sensitive to β-ionone and hexanal (Fig. 2c), but not to hexanoic acid. Therefore, these results demonstrated that the different OBPs conserved their activities and their specificity towards a range of VOCs even after the addition of a cysteine residue at their N-terminal end and their immobilization onto the prism.

On top of that, the kinetic responses obtained with β-ionone were different from those obtained with hexanal. For example, hexanal gave a more intense effective signal on the biosensors based on OBP3-a than on the ones based on OBP3-w, which is consistent with the ITC measurements. The binding of hexanal to OBP3-a was also much quicker than its binding to OBP3-w. These results confirmed that the modification of the binding pocket of OBP3-a yielded new binding properties, which were preserved after immobilization of the proteins onto the prism. Moreover, these kinetic features could be useful for the discrimination between different VOC families, for instance using principal component analysis based on kinetic models (Genua et al., 2014).

In all the cases, the variation of reflectivity was low ($< 0.15\%$). It was expected that a detection of VOCs using SPRi would give rather low signal. To determine whether it is possible to obtain such a variation simply by virtue of the binding of the VOCs on a monolayer of OBPs, we made a comparison with the typical variation obtained for the detection of biomolecules by SPRi in literature. For instance, an adsorbed layer of thrombin (37 kDa) gave rise to a variation of reflectivity of 6–7% on an aptamer chip (Daniel et al., 2013). A reflectivity increase of about 1% was found with the ligation of a DNA fragment (6 kDa) (Lu et al., 2017a). Extrapolating to VOC detection (200 g/mol), it is expected to obtain a reflectivity variation around $[0.03 \pm 0.01]$ %. In fact, the observed signal intensity is much higher.

Since SPR is very sensitive to the optical properties of the sensing layer on the prism surface, any phenomena having impact on the local refractive index, which are not due to direct mass addition, can be observed (Sota et al., 1998). In particular, in the field of biosensors, such phenomena can amplify the SPR signal. For instance, Miyazaki and his collaborators successfully detected uric acid and glucose despite their small size through the variation of polarization of specific

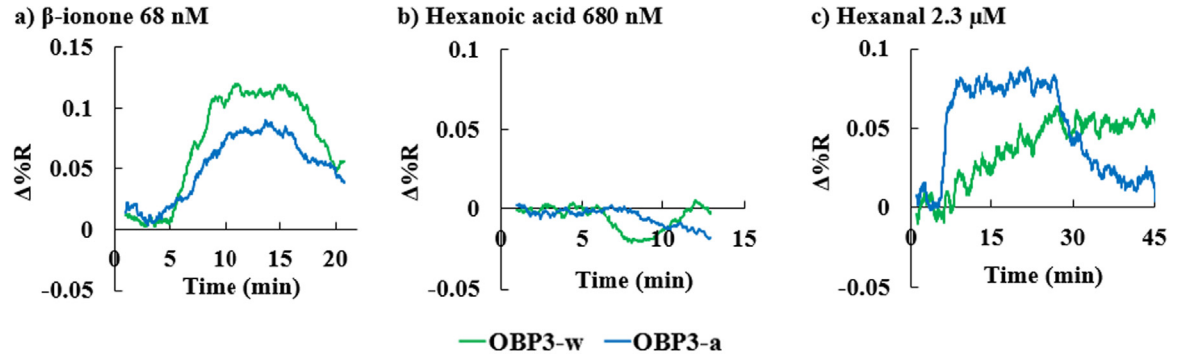

Fig. 2. Sensorgrams showing kinetic responses of the two active OBPs after exposure to a) β-ionone, b) hexanoic acid and c) hexanal. The average reflectivity obtained with the biosensors based on OBP3-c was subtracted to the signals of the ones based on OBP3-w and OBP3-a.

enzymes (Miyazaki et al., 2017). More interestingly, the conformational change of immobilized proteins after the binding of a ligand may result in a modification of their hydrodynamic radius (Gestwicki et al., 2001) and, consequently, a variation of the refractive index. It enabled the detection of targets as small as calcium ions (40 Da), in a dynamic way (Dell'Orco et al., 2012) by SPR and SPRi (Kim et al., 2005). All these small molecular mass ligands would not give valid signals with these methods if only based on mass variation on the sensor.

To our knowledge, no study has been led on the conformational change that could occur in the rat OBP3 upon ligand binding. Nespoulous and collaborators showed that ligand binding induces local structural change in the rat OBP-1F (Nespoulous et al., 2004). Slight shifts of tyrosine residues are likely to induce a rearrangement of the protein backbone, which modifies its circular dichroism spectrum. This experimental observation was confirmed by molecular dynamics simulations, implying that in the presence of a ligand, a strand pair separation yields to an "open barrel" conformational state (Hajjar et al., 2006). If we cannot assert that the same type of behavior is observed for OBP3-w and OBP3-a solely based on the results presented here, we hypothesized that the binding of VOCs to the active OBPs most likely induced a conformational change of the proteins. Such a change would give rise to a variation of local refractive index detectable by SPRi. Further characterization will be needed to confirm it.

Furthermore, in order to check if these signals were reliable, the effective signals obtained with the three olfactory biosensors after exposure to β-ionone, hexanal, and hexanoic acid were presented in Fig. 3, together with their corresponding SNR values. Satisfyingly, the SNR calculated for the responses of the biosensors based on OBP3-w and OBP3-a to β-ionone and hexanal was greater than three. Therefore, these results confirmed that SPRi is efficient for the direct detection of VOCs and for the development of novel olfactory biosensors.

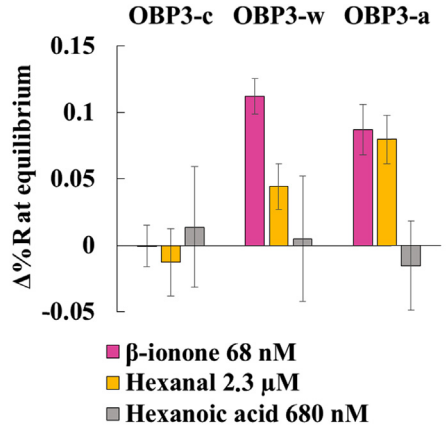

SNR	OBP3-c	OBP3-w	OBP3-a
β-ionone	0.01	8.33	4.55
Hexanal	0.50	2.56	4.37
Hexanoic acid	0.31	0.11	0.46

Fig. 3. Effective signals obtained with the three olfactory biosensors after exposure to β-ionone, hexanal, and hexanoic acid. The corresponding SNR values are presented in the table below.

3.3. Sensitivity and selectivity of the olfactory biosensors

In order to evaluate the sensitivity of the olfactory biosensors to β-ionone, a set of measurements was performed using different concentrations ranging from 10 pM to 68 nM. The minimum concentration detected with a valid signal (SNR > 3) was 200 pM (Fig. 1b), which was validated on at least three different microarrays. However, it was found that the signal intensity was not proportional to the VOC concentration. In fact, for the concentrations above 200 pM, valid signals were obtained but with comparable intensity.

In literature, most of the OBP-based biosensors used for the detection of VOCs in solution have a limit of detection in the micro-molar range. Therefore, the limit of detection obtained with our olfactory biosensors is among the lowest ones. Zhang et al. (2015) obtained a limit of detection of 26.7 pM for β-ionone using insect OBPs and localized surface plasmon resonance as a transduction method. However, this value was extrapolated from the calibration curve as the concentration corresponding to 3 times the noise of detection and the lowest concentration tested was 10 nM. More recently, Lu and collaborators (Lu et al., 2017b) developed an olfactory biosensor using human OBPs based on electrochemical cyclic voltammetry for the detection of aldehydes and fatty acids. The concentrations tested ranged from 5 pM to 500 nM. They estimated a limit of detection, once again by calculation, around 0.5 pM.

Furthermore, it is particularly remarkable that our olfactory biosensors based on SPRi are able to detect these small VOCs in solution, especially at such low concentrations. The limit of detection in mass commonly admitted for commercial SPRi apparatus is 200 g/mol, without any amplification (Campbell and Kim, 2007). Herein, we obtained a valid signal with hexanal, which has a molecular weight of 100 g/mol. On top of that, an analyte concentration above $K_d/1000$ is generally required to obtain a reliable signal without signal amplification in SPRi. Yet, a valid signal was observed using a concentration at $K_d/5000$ for the binding of β-ionone to OBP3-w. This is purely indicative since the K_d on chip probably differs from the K_d in solution. Nevertheless, these results supported our hypothesis that the reflectivity variation is not simply due to the binding of the VOCs to the OBPs, but rather to the conformational change of the proteins, which acts as an amplifier. As a result, the linear range of the sensor is shifted to lower concentrations of VOCs. Furthermore, the relatively high

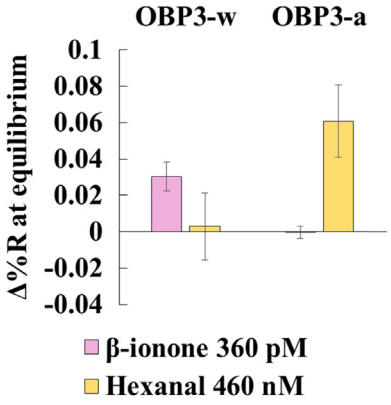

SNR	OBP3-w	OBP3-a
β-ionone	3.74	0.091
Hexanal	0.163	3.06

Fig. 4. Effective signals obtained with the two active olfactory biosensors after exposure to β-ionone and hexanal at low concentrations, showing their high sensitivity and selectivity. The corresponding SNR values are presented in the table below.

amplitude of the noise narrows the measurable part of this linear range of concentrations from 100 pM to 1 nM, which is unsuitable for the quantitative detection of VOCs. Improvements to the sensors will be needed to increase the signal-to-noise ratio so as to construct a calibration curve.

Concerning the selectivity, as shown in Fig. 3, at relatively high concentration, β-ionone bound to the two olfactory biosensors with a higher affinity for the OBP3-w-based olfactory biosensor. In contrast, hexanal bound preferentially to the biosensor based on OBP3-a. This is consistent with the results obtained in solution by ITC measurements. Most importantly, it was observed that at much lower VOC concentrations, the biosensors exhibited an extremely high selectivity (Fig. 4). Indeed, at 360 pM β-ionone bound only to the olfactory biosensors based on OBP3-w. Similarly, at 460 nM, hexanal bound only to the OBP3-a-based biosensor. All these results demonstrate that our olfactory biosensors are relevant for the trace detection with a high selectivity, rather than for quantitative analysis of VOCs.

3.4. Optimized regeneration procedures for the improvement of biosensor performances

As mentioned before, OBPs can reversibly bind VOCs with dissociation constants in the micro-molar range. In this study, after the injection of β-ionone at relatively low concentrations (< 800 pM), it was sufficient to keep the buffer solution running to obtain a complete regeneration of the two active olfactory biosensors. In this case, the reflectivity went back spontaneously to its original baseline in 25 min (see Fig. S2a in Supplementary material). The microarray was subsequently re-used to analyze other samples up to 12 consecutive injections of β-ionone in a row, with a SNR above 3.

However, after an injection at a concentration above 800 pM and a spontaneous regeneration, the signal did not go back exactly to the baseline and a subsequent loss of signal intensity was observed. For instance, at 6.8 nM, the signal decreased to about half of its intensity (see Fig. S2a in Supplementary material).

In fact, after an injection of β-ionone at high concentrations or after an injection of hexanal, this process did not allow a complete regeneration of the microarray. Therefore, a new strategy was developed, taking inspiration from the purification method used after the production of OBPs (Barou et al., 2015). The idea was to put OBPs in contact with organic solvents such as ethanol and acetonitrile. It allowed, on the one hand, to slightly and reversibly denature the proteins and thus unfold their binding pocket; on the other hand, to solubilize the VOCs and facilitate their evacuation out of this binding pocket. After this procedure, when back in phosphate buffer, the OBPs recovered their original structure and activity. All this procedure was carried out directly in situ in the SPR chamber, using the fluidic system to convey the solvents to the OBP-based biosensors (see Fig. S1 in Supplementary material). The complete regeneration took 90 min.

This procedure was very efficient for all the VOCs tested, even at high concentrations. Thanks to it, our olfactory biosensors demonstrated a very good repeatability from measurement to measurement. For instance, we obtained a signal at equilibrium of [0.07 ± 0.01]%, for 9 injections of β-ionone in a row at 68 nM (see Fig. S2b in Supplementary material). Moreover, the lifespan of the olfactory biosensors was increased to about two months, which is remarkable, compared to other olfactory biosensors in literature. The repeatability from chip to chip, assessed by injections of β-ionone, was also good on 8 chips (not shown).

4. Conclusions

In this work, derivatives of OBPs with customized binding properties were used for the first time, in association with an optical transduction system, SPRi, to develop olfactory biosensors. Under optimized deposition conditions, we showed that OBPs directly immobilized on the chip retained their activity. These biosensors were promising for highly sensitive and selective analysis of VOCs in solution. First of all, the detection limits both in concentration (200 pM of β-ionone) and in molecular weight of VOCs (100 g/mol for hexanal) are among the lowest in literature. A valid signal was obtained in both cases. The intensities of the signals could not be explained solely by the mass increase after adsorption of VOCs on the protein layer. We therefore hypothesized that the binding of VOCs to OBPs induced a conformational change, which led to a variation in the local refractive index and amplified the SPRi signals. Moreover, the distinct binding properties of the OBP derivatives enabled very high selectivity at low concentrations of VOCs. Finally, different regeneration strategies were established. With appropriate regeneration procedures, these biosensors showed good repeatability not only from measurement-to-measurement but also from chip-to-chip, as well as good stability with a lifespan of up to nearly two months.

However, the lifespan of these biosensors remains intrinsically limited by the use of proteins. Besides, the narrow observable part of linear range (from 100 pM to 1 nM for β-ionone) is not appropriate for the quantitative analysis of VOCs. Future work will be done on the passivation of the chip surface to limit non-specific adsorption so as to reduce the noise. A rational surface chemistry could also be developed to stabilize the protein layer and so increase the lifespan of the biosensors. Finally, this work showed that the design of new OBPs tailored to specifically target VOCs allows a gain of sensitivity and selectivity. Protein engineering could help to increase their robustness. This work may pave the way for the design and use of new custom-made olfactory proteins to specifically target a wider range of VOCs with high societal impact.

Acknowledgements

The Ph.D. thesis of C. Hurot is financially supported by the French Alternative Energies and Atomic Energy Commission (CEA), France. The Ph.D. thesis of S. Brenet is co-funded by the French Defense Procurement Agency (DGA), France and CEA. The Ph.D. thesis of E. Barou is funded by the French Ministry of Higher Education and Research, France. SyMMES laboratory is part of Labex Arcane program (ANR-12-LABX-003) and Labex LANEF program (ANR-10-LABX-51-01). Both Arcane and LANEF were funded by the French National

Research Agency, France.

Conflict of interest

The authors declare no competing financial interest.

Appendix A. Supplementary material

Supplementary data associated with this article can be found in the online version at doi:10.1016/j.bios.2018.08.072.

References

Barou, E., Sigoillot, M., Bouvet, M., Briand, L., Meunier-Prest, R., 2015. Electrochemical detection of the 2-isobutyl-3-methoxypyrazine model odorant based on odorant-binding proteins: the proof of concept. Bioelectrochemistry 101 (Suppl. C), 28–34.

Campbell, C.T., Kim, G., 2007. SPR microscopy and its applications to high-throughput analyses of biomolecular binding events and their kinetics. Biomaterials 28 (15), 2380–2392.

Cannatà, D., Benetti, M., Verona, E., Varriale, A., Staiano, M., Auria, S.D., Di Pietrantonio, F., 2012. Odorant detection via solidly mounted resonator biosensor. In: Proceedings of the 2012 IEEE International Ultrasonics Symposium, pp. 1537–1540.

Chiu, S.W., Tang, K.T., 2013. Towards a chemiresistive sensor-integrated electronic nose: a review. Sensors 13 (10), 14214–14247.

Daniel, C., Mélaïne, F., Roupioz, Y., Livache, T., Buhot, A., 2013. Real time monitoring of thrombin interactions with its aptamers: insights into the sandwich complex formation. Biosens. Bioelectron. 40 (1), 186–192.

Dell'Orco, D., Sulmann, S., Linse, S., Koch, K.-W., 2012. Dynamics of conformational Ca2+-switches in signaling networks detected by a planar plasmonic device. Anal. Chem. 84 (6), 2982–2989.

Di Pietrantonio, F., Cannatà, D., Benetti, M., Verona, E., Varriale, A., Staiano, M., D'Auria, S., 2013. Detection of odorant molecules via surface acoustic wave biosensor array based on odorant binding proteins. Biosens. Bioelectron. 41, 328–334.

Du, L., Wu, C., Liu, Q., Huang, L., Wang, P., 2013. Recent advances in olfactory receptor-based biosensors. Biosens. Bioelectron. 42 (1), 570–580.

Genua, M., Garçon, L.-A., Mounier, V., Wehry, H., Buhot, A., Billon, M., Calemczuk, R., Bonnaffé, D., Hou, Y., Livache, T., 2014. SPR imaging based electronic tongue via landscape images for complex mixture analysis. Talanta 130, 49–54.

Gestwicki, J.E., Hsieh, H.V., Pitner, J.B., 2001. Using receptor conformational change to detect low molecular weight analytes by surface plasmon resonance. Anal. Chem. 73 (23), 5732–5737.

Gomila, G., Casuso, I., Errachid, A., Ruiz, O., Pajot, E., Minic, J., Gorojankina, T., Persuy, M.A., Aioun, J., Salesse, R., Bausells, J., Villanueva, G., Rius, G., Hou, Y., Jaffrezic, N., Pennetta, C., Alfinito, E., Akimov, V., Reggiani, L., Ferrari, G., Fumagalli, L., Sampietro, M., Samitier, J., 2006. Advances in the production, immobilization, and electrical characterization of olfactory receptors for olfactory nanobiosensor development. Sens. Actuators B: Chem. 116 (1), 66–71.

Hajjar, E., Perahia, D., Debat, H., Nespoulous, C., Robert, C.H., 2006. Odorant binding and conformational dynamics in the odorant-binding protein. J. Biol. Chem. 281 (40), 29929–29937.

Heydel, J.M., Coelho, A., Thiebaud, N., Legendre, A., Bon, A.M.L., Faure, P., Neiers, F., Artur, Y., Golebiowski, J., Briand, L., 2013. Odorant-binding proteins and xenobiotic metabolizing enzymes: implications in olfactory perireceptor events. Anat. Rec. 296 (9), 1333–1345.

Homola, J., 2008. Surface plasmon resonance sensors for detection of chemical and biological species. Chem. Rev. 108 (2), 462–493.

Hou, C.J., Dong, J.L., Qin, H., Huo, D.Q., Shen, C.H., 2012a. Development of cell-based olfactory biosensors. Anal. Lett. 45 (2–3), 202–218.

Hou, Y., Jaffrezic-Renault, N., Martelet, C., Tlili, C., Zhang, A., Pernollet, J.-C., Briand, L., Gomila, G., Errachid, A., Samitier, J., Salvagnac, L., Torbiero, B., Temple-Boyer, P., 2005. Study of Langmuir and Langmuir-Blodgett films of odorant-binding protein/amphiphile for odorant biosensors. Langmuir 21, 4058–4065.

Hou, Y., Jaffrezic-Renault, N., Martelet, C., Zhang, A., Minic-Vidic, J., Gorojankina, T., Persuy, M.-A., Pajot-Augy, E., Salesse, R., Akimov, V., Reggiani, L., Pennetta, C., Alfinito, E., Ruiz, O., Gomila, G., Samitier, J., Errachid, A., 2007. A novel detection strategy for odorant molecules based on controlled bioengineering of rat olfactory receptor I7. Biosens. Bioelectron. 22 (7), 1550–1555.

Hou, Y., Genua, M., Tada Batista, D., Calemczuk, R., Buhot, A., Fornarelli, P., Koubachi, J., Bonnaffé, D., Saesen, E., Laguri, C., Lortat-Jacob, H., Livache, T., 2012b. Continuous evolution profiles for electronic-tongue-based analysis. Angew. Chem. 124 (41), 10540–10544.

Hou, Y., Genua, M., Garcon, L.A., Buhot, A., Calemczuk, R., Bonnaffe, D., Lortat-Jacob, H., Livache, T., 2014. Electronic tongue generating continuous recognition patterns for protein analysis. J. Vis. Exp.: JoVE 91, 51901.

Kim, M., Jung, S.O., Park, K., Jeong, E.J., Joung, H.A., Kim, T.H., Seol, D.W., Chung, B.H., 2005. Detection of Bax protein conformational change using a surface plasmon resonance imaging-based antibody chip. Biochem. Biophys. Res. Commun. 338 (4), 1834–1838.

Kotlowski, C., Larisika, M., Guerin, P.M., Kleber, C., Kröber, T., Mastrogiacomo, R., Nowak, C., Pelosi, P., Schütz, S., Schwaighofer, A., Knoll, W., 2018. Fine discrimination of volatile compounds by graphene-immobilized odorant-binding proteins. Sens. Actuators B: Chem. 256, 564–572.

Larisika, M., Kotlowski, C., Steininger, C., Mastrogiacomo, R., Pelosi, P., Schütz, S., Peteu, S.F., Kleber, C., Reiner-Rozman, C., Nowak, C., Knoll, W., 2015. Electronic olfactory sensor based on A. mellifera odorant-binding protein 14 on a reduced graphene oxide field-effect transistor. Angew. Chem. 127, 13443–13446.

Lee, S.H., Oh, E.H., Park, T.H., 2015. Cell-based microfluidic platform for mimicking human olfactory system. Biosens. Bioelectron. 74, 554–561.

Liu, Q.J., Ye, W.W., Xiao, L.D., Du, L.P., Hu, N., Wang, P., 2010. Extracellular potentials recording in intact olfactory epithelium by microelectrode array for a bioelectronic nose. Biosens. Bioelectron. 25 (10), 2212–2217.

Löbel, D., Jacob, M., Völkner, M., Breer, H., 2002. Odorants of different chemical classes interact with distinct odorant binding protein subtypes. Chem. Senses 27 (1), 39–44.

Lu, C., Saint-Pierre, C., Gasparutto, D., Roupioz, Y., Peyrin, E., Buhot, A., 2017a. Linear chain formation of split-aptamer dimers on surfaces triggered by adenosine. Langmuir 33 (44), 12785–12792.

Lu, Y., Zhang, D., Zhang, Q., Huang, Y., Luo, S., Yao, Y., Li, S., Liu, Q., 2016. Impedance spectroscopy analysis of human odorant binding proteins immobilized on nanopore arrays for biochemical detection. Biosens. Bioelectron. 79, 251–257.

Lu, Y., Huang, Y., Li, S., Zhang, Q., Wu, J., Xiong, Z., Xiong, L., Wan, Q., Liu, Q., 2017b. Fat taste detection with odorant-binding proteins (OBPs) on screen-printed electrodes modified by reduced graphene oxide. Sens. Actuators B: Chem. 252, 973–982.

Lu, Y., Yao, Y., Li, S., Zhang, Q., Liu, Q., 2017c. Olfactory biosensor based on odorant-binding proteins of Bactrocera dorsalis with electrochemical impedance sensing for pest management. Sens. Rev. 37 (4), 396–403.

Maillart, E., Livache, T., Leroy, L., 2012. Biological Applications of Surface Plasmon Resonance Imaging.

Manai, R., Scorsone, E., Rousseau, L., Ghassemi, F., Possas Abreu, M., Lissorgues, G., Tremillon, N., Ginisty, H., Arnault, J., Tuccori, E., Bernabei, M., Cali, K., Persaud, K., Bergonzo, P., 2014. Grafting odorant binding proteins on diamond bio-MEMS. Biosens. Bioelectron. 60, 311–317.

Miyazaki, C.M., Shimizu, F.M., Mejía-Salazar, J.R., Oliveira, O.N., Ferreira, M., 2017. Surface plasmon resonance biosensor for enzymatic detection of small analytes. Nanotechnology 28 (14).

Mulla, M.Y., Tuccori, E., Magliulo, M., Lattanzi, G., Palazzo, G., Persaud, K., Torsi, L., 2015. Capacitance-modulated transistor detects odorant binding protein chiral interactions. Nat. Commun. 6, 6010.

Nespoulous, C., Briand, L., Delage, M.-M., Tran, V., Pernollet, J.-C., 2004. Odorant binding and conformational changes of a rat odorant-binding protein. Chem. Senses 29 (3), 189–198.

Pelosi, P., Mastrogiacomo, R., Iovinella, I., Tuccori, E., Persaud, K.C., 2014. Structure and biotechnological applications of odorant-binding proteins. Appl. Microbiol. Biotechnol. 98 (1), 61–70.

Sota, H., Hasegawa, Y., Iwakura, M., 1998. Detection of conformational changes in an immobilized protein using surface plasmon resonance. Anal. Chem. 70 (10), 2019–2024.

Tcatchoff, L., Nespoulous, C., Pernollet, J.C., Briand, L., 2006. A single lysyl residue defines the binding specificity of a human odorant-binding protein for aldehydes. FEBS Lett. 580 (8), 2102–2108.

Wang, S., Shan, X., Patel, U., Huang, X., Lu, J., Li, J., Tao, N., 2010. Label-free imaging, detection, and mass measurement of single viruses by surface plasmon resonance. Proc. Natl. Acad. Sci. USA 107 (37), 16028–16032.

Wasilewski, T., Gebicki, J., Kamysz, W., 2017. Bioelectronic nose: current status and perspectives. Biosens. Bioelectron. 87, 480–494.

Wasilewski, T., Gębicki, J., Kamysz, W., 2018. Advances in olfaction-inspired biomaterials applied to bioelectronic noses. Sens. Actuators B: Chem. 257, 511–537.

Zhang, D., Lu, Y., Zhang, Q., Yao, Y., Li, S., Li, H., Zhuang, S., Jiang, J., Liu, G.L., Liu, Q., 2015. Nanoplasmonic monitoring of odorants binding to olfactory proteins from honeybee as biosensor for chemical detection. Sens. Actuators B: Chem. 221, 341–349.